



# Validation of brightness and physical temperature from two scanning microwave radiometers in the 60 GHz O<sub>2</sub> band using radiosonde measurements

Francisco Navas-Guzmán<sup>1</sup>, Niklaus Kämpfer<sup>1</sup>, and Alexander Haefele<sup>2</sup>

<sup>1</sup>Institute of Applied Physics (IAP), University of Bern, Bern, Switzerland

<sup>2</sup>Federal Office of Meteorology and Climatology MeteoSwiss, Payerne, Switzerland

Correspondence to: Francisco Navas-Guzmán (francisco.navas@iap.unibe.ch)

Received: 6 March 2016 – Published in Atmos. Meas. Tech. Discuss.: 29 March 2016

Revised: 31 August 2016 – Accepted: 5 September 2016 – Published: 20 September 2016

**Abstract.** In this paper, we address the assessment of the tropospheric performance of a new temperature radiometer (TEMPERA) at 60 GHz. With this goal, an intercomparison campaign was carried out at the aerological station of MeteoSwiss in Payerne (Switzerland). The brightness temperature and the tropospheric temperature were assessed by means of a comparison with simultaneous and collocated radiosondes that are launched twice a day at this station. In addition, the TEMPERA performances are compared with the ones from a commercial microwave radiometer (HATPRO), which has some different instrumental characteristics and uses a different inversion algorithm. Brightness temperatures from both radiometers were compared with the ones simulated using a radiative transfer model and atmospheric profiles from radiosondes. A total of 532 cases were analyzed under all weather conditions and evidenced larger brightness temperature deviations between the two radiometers and the radiosondes for the most transparent channels. Two different retrievals for the TEMPERA radiometer were implemented in order to evaluate the effect of the different channels on the temperature retrievals. The comparison with radiosondes evidenced better results very similar to the ones from HATPRO, when the eight more opaque channels were used. The study shows the good performance of TEMPERA to retrieve temperature profiles in the troposphere. The inversion method of TEMPERA is based on the optimal estimation method. The main advantage of this algorithm is that there is no necessity for radiosonde information to achieve good results in contrast to conventional methods as neural networks or lineal regression. Finally, an assessment of the effect of instrumental characteristics as the filter response and the antenna pattern

on the brightness temperature showed that they can have an important impact on the most transparent channels.

## 1 Introduction

The importance of the knowledge of the thermal structure for scientific understanding of atmospheric processes is widely recognised. The air temperature plays a crucial role on the dynamical, chemical and radiative processes in the atmosphere. In the lowest part of the atmosphere, temperature profiles are a key input for the weather forecast models. Techniques based on in situ or remote sensing measurements are used nowadays to measure atmospheric temperature profiles. Among the in situ techniques, radiosondes (RSs) are extensively used due to high vertical resolution.

Recently, the global Aircraft Meteorological Data Relay (AMDAR) programme initiated by the World Meteorological Organization (WMO) and its members has been using aircraft temperature measurements for a range of meteorological applications (public weather forecasting, climate monitoring and prediction, etc). The aircraft use sensors or the emerging MODE-S method to retrieve the temperature (De Haan, 2011).

Other measurement techniques have become available to address the necessity of temperature measurements in the troposphere and in the stratosphere. These measurements include lidar and microwave radiometers.

Microwave radiometers present the main advantage of having the capacity of providing atmospheric profiles with

a high temporal resolution and a reasonable vertical resolution. In addition, long-term measurements in a fixed location allow the local atmospheric thermodynamics to be characterised.

At present there are different configurations of ground-based microwave radiometers to measure tropospheric temperature profiles; some examples are MICCY (Microwave Radiometer for Cloud Cartography) (Crewell et al., 2001), Radiometrics MP-3000A (Ware et al., 2003), RPG-HATPRO (Radiometer Physics GmbH – Humidity and Temperature Profiler) (Rose et al., 2005) and ASMUWARA (All-Sky MultiWavelength Radiometer) (Martin et al., 2006).

A relatively new temperature radiometer (TEMPERA) has been designed and built by the microwave group at the Institute of Applied Physics (IAP), University of Bern, Switzerland. This is the first ground-based radiometer that measures temperature profiles in the troposphere and in the stratosphere simultaneously (Stähli et al., 2013; Navas-Guzmán et al., 2014).

The presented study aims to assess the tropospheric performance of the TEMPERA radiometer, and compares it with independent in situ radiosonde measurements. TEMPERA has also been compared with a commercial microwave radiometer (HATPRO) manufactured by Radiometer Physics GmbH, Germany (RPG). This second radiometer has some different technical characteristics, and the inversion algorithm is based on a different method. Most of the temperature inversion algorithms used for commercial radiometers are based on neural networks or linear regression methods, which are disadvantaged by the need to use radiosondes to train that method. The difficulty in the availability of a statistically significant radiosonde database for the location of the microwave radiometer is one of the major drawbacks of these methods. In this sense, TEMPERA's inversion algorithm based on the optimal estimation method (OEM) (Rodgers, 2000) overcomes this problem. In addition to the temperature assessment, the radiances measured from both radiometers (brightness temperatures) will be evaluated. For that purpose the brightness temperature ( $T_b$ ) from both radiometers are compared with the simulated  $T_b$  from radiosondes using a radiative transfer model. Finally, this study also aims to assess how some instrumental characteristics as the filter response and the antenna pattern affect the measured radiances (brightness temperature).

The paper has been organised in the following way. Section 2 presents the experimental site and the instrumentation used in this study. Section 3 describes the methodology of the radiative transfer model and the temperature inversions. Sections 4 and 5 present the brightness and physical temperature comparisons carried out for 1 year of measurements. An assessment of the effect of radiometer characteristics as the filter response and the antenna pattern on the brightness temperature is presented in Sect. 6. Finally the conclusions are found in Sect. 7.

## 2 Experimental site and instrumentation

A special campaign has been set up at the aerological station in Payerne (46.82° N, 6.95° E; 491 m above sea level) of the Swiss Federal Institute of Meteorology and Climatology (MeteoSwiss). For this campaign, the TEMPERA radiometer was moved from the ExWi building of the University of Bern (Bern, Switzerland) to Payerne in December 2013. The main goal of this campaign is to assess the tropospheric and stratospheric performance of TEMPERA using the versatile instrumentation available at this MeteoSwiss station. Particularly, in this study we will assess the brightness temperature and the tropospheric temperature profiles, comparing them with the radiosondes, which are launched twice a day at this station. In addition, the performance of TEMPERA is compared with another microwave radiometer (HATPRO), which has some different instrumental characteristics and also uses a different inversion algorithm. The pointing directions for TEMPERA and HATPRO radiometers during the campaign are northwest (320°) and north (350°), respectively. Next a technical description of the different instruments used in this study is presented.

The temperature radiometer called TEMPERA has been designed and built by the Institute of Applied Physics (IAP) of the University of Bern (Stähli et al., 2013). Figure 1 shows a picture of this radiometer at the laboratory at ExWi, Bern (Switzerland). TEMPERA is a heterodyne receiver that covers the frequency range of 51–57 GHz. The instrument consists of a front end to collect the microwave radiation and two back ends for the detection (a filter bank and a fast Fourier transform spectrometer; FFT). The incoming radiation is directed into a corrugated horn antenna using an off-axis parabolic mirror. The antenna is characterised by a half-power beamwidth (HPBW) of 4°. The calibration of the detected signal in the two back ends is performed by means of an ambient hot load in combination with a noise diode. The brightness temperature accuracy for this radiometer is 0.5 K, and the radiometric resolution is between 0.03 and 0.05 K for 1.0 s integration time (Stähli et al., 2013).

The tropospheric measurements in TEMPERA are performed using the filter bank. It consists of 4 filters which are able to measure at 12 frequencies by tuning the frequency of a local oscillator with a synthesizer. Thus, the positions between the emission lines in the 51–57 GHz range are covered uniformly (see Fig. 2). Filters with different bandwidths are used to measure at the 12 frequencies; while for 9 lower channels the filters' bandwidths are 250 GHz, for the 3 more opaque channels (10–12) wider ones (1 GHz) are used in order to enhance the sensitivity in the flat spectral region. Table 1 shows the central frequencies and the bandwidths of all the channels. For tropospheric measurements a scan is performed by TEMPERA in every measurement cycle, covering the elevation angle range from 20 to 60° in steps of 5° (nine angles). Crewell and Lohnert (2007) showed that these elevation scanning measurements increase the accuracy of the

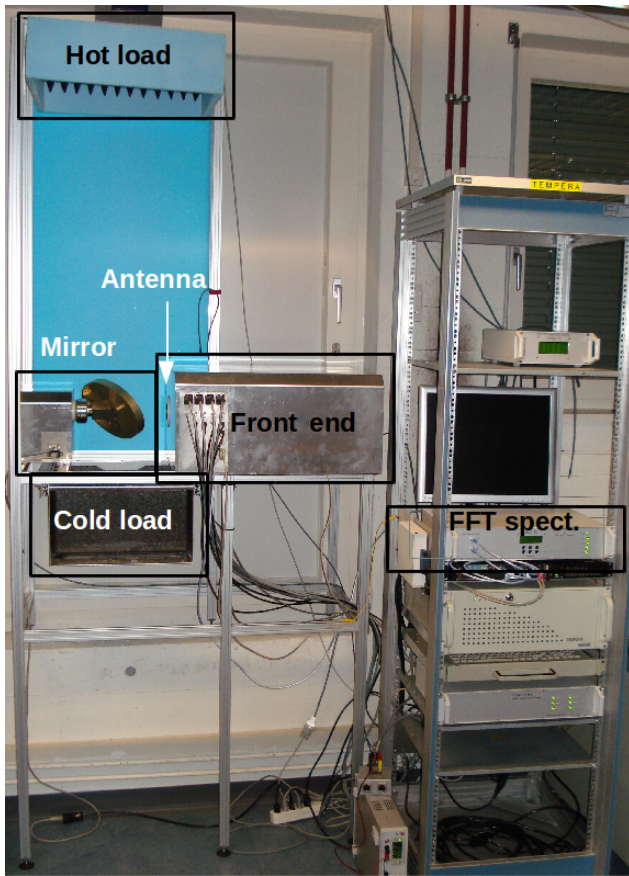


**Figure 1.** TEMPERA at the laboratory at ExWi, Bern (Switzerland).

retrieved temperature, specifically in the boundary layer, for microwave radiometers.

For the stratospheric temperature retrievals, TEMPERA uses the second back end (FFT spectrometer, Acquiris AC 240) to measure the two oxygen emission lines centred at 52.5424 and 53.0669 GHz. Stratospheric measurements are not treated in this paper, and a detailed description of this other measurement mode can be found in Stähli et al. (2013) and Navas-Guzmán et al. (2015).

TEMPERA performs periodic measurement cycles of 60 s. Each cycle starts with a hot load calibration in combination with a noise diode followed by the atmosphere measurements (scanning from 60 to 20° elevation angle in steps of 5°). After calibration, the output of each measurement cycle is a set of 108 brightness temperatures corresponding to the 12 frequencies and the 9 elevation angles. The noise diode is calibrated regularly (about once a month) using a cold load (liquid nitrogen) and a hot load (ambient). The time resolution of these retrievals is 15 min (Stähli et al., 2013).

The other microwave radiometer used in the study is a HATPRO radiometer (RPG-HATPRO, Radiometer Physics GmbH) (Rose et al., 2005). This instrument provides very accurate values of liquid water path (LWP) and integrated

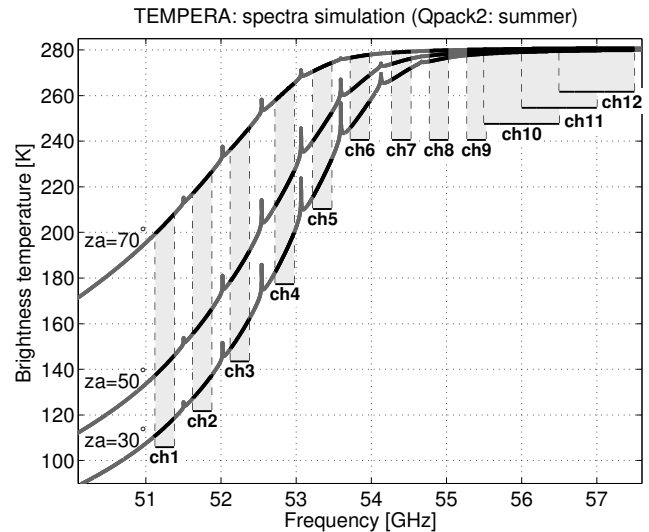


**Figure 2.** Simulated brightness temperatures using ARTS model for the TEMPERA radiometer at different zenith angles (30, 50 and 70°). The grey bars indicate the 12 channels of the filter bank.

**Table 1.** Frequencies ( $f$ ) and bandwidths ( $B$ ) of TEMPERA’s tropospheric channels (ch1–ch12).

Channel	$f$ (GHz)	$B$ (MHz)	Channel	$f$ (GHz)	$B$ (MHz)
1	51.25	250	7	54.40	250
2	51.75	250	8	54.90	250
3	52.25	250	9	55.40	250
4	52.85	250	10	56.00	1000
5	53.35	250	11	56.50	1000
6	53.85	250	12	57.00	1000

water vapour (IWV) with a high temporal resolution (1 s). Measurements in the bands 22–31 and 51–58 GHz make it possible to retrieve humidity and temperature profiles with this radiometer.

HATPRO measures the sky brightness temperature at six elevation angles (90.0, 42.0, 30.0, 19.2, 10.2 and 5.4°) corresponding to 1.0, 1.5, 2.0, 3.0, 5.6 and 10.6 air masses in a continuous and automated way with a radiometric accuracy between 0.3 and 0.4 K root mean square error at 1.0 s integration time.

Whereas the first band provides highly accurate information of humidity and cloud liquid water content (Löhnert and Crewell, 2003), the second band contains information about the tropospheric vertical structure of the temperature due to the homogeneous mixing of O<sub>2</sub> (Crewell and Löhnert, 2007). HATPRO uses two filter banks in order to detect the radiation coming from both bands in parallel. For temperature retrievals seven channels are used at the frequencies of 51.26, 52.28, 53.86, 54.94, 56.66, 57.30 and 58.00 GHz. The lower four channels have a bandwidths of 230 MHz, while for the optically thick channels (56.66–58 GHz) wider bandwidths (2 GHz) are used. The temperature profiles from HATPRO

are averaged in order to get the same temporal resolution as for the TEMPERA radiometer (15 min).

Independent in situ temperature measurements are taken by means of radiosondes. Radiosondes have been regularly launched twice a day at the aerological station of Payerne since 1954. They typically reach altitudes around 30 km, with a vertical resolution that ranges between 10 and a maximum of 80 m, with a highest resolution in the first part of the flight. The sensors of these radiosondes include copper–constantan thermocouples for temperature, a full range water hygrosonde for pressure and a carbon hygrometer for relative humidity. The accuracy of these three parameters in the troposphere is  $\pm 0.2$  K for temperature,  $\pm 2$  hPa (accuracy increases with height) for pressure and  $\pm 5$  to 10 % for relative humidity (Löhnert and Maier, 2012).

As it was indicated before, the microwave radiometer retrievals have been averaged over 15 min. We consider that this time resolution is good enough to compare with radiosondes since it is the average time that a radiosonde can reach altitudes around 4–5 km, which is the range in which microwave radiometers have their maximum response (higher measurement response). In addition, any change in the atmospheric conditions during this time interval would be much more pronounced in the lower part of the troposphere than in the upper part.

### 3 Methodology

TEMPERA and HATPRO radiometers measure thermal radiation in the range from 51 to 58 GHz coming from the wing of the 60 GHz oxygen emission region. For a well-mixed gas such as oxygen, whose fractional concentration is altitude-independent below 80 km, the radiation firstly provides information on atmospheric temperature.

A microwave radiometer measures atmospheric thermal emissions coming from different altitudes. The intensity of the radiation detected at ground level can be calculated as a function of the frequency-dependent microwave brightness temperature ( $T_b$ ). Under the Rayleigh–Jeans approximation ( $h\nu \ll kT$ ) the radiative transfer equation (RTE) is expressed as

$$T_b(h_0, \theta) = T_0 e^{-\tau(h_1, \theta)} + \int_{h_0}^{h_1} T(h) e^{-\tau(h, \theta)} \alpha \frac{1}{\sin(\theta)} dh, \quad (1)$$

where  $T_b(\theta)$  is the brightness temperature at elevation angle  $\theta$ ,  $T_0$  is the brightness temperature of the cosmic background radiation,  $T(h)$  is the physical temperature at height  $h$ ,  $h_0$  is the altitude at ground,  $h_1$  is an upper boundary in the atmosphere,  $\alpha$  is the absorption coefficient and  $\tau$  is the opacity. The opacity is defined as

$$\tau(h, \theta) = \int_{h_0}^h \alpha(h') \frac{1}{\sin(\theta)} dh'. \quad (2)$$

The estimated brightness temperature can easily be calculated from Eq. 1 by just knowing the state of the atmosphere (forward model). However, a much more complex task is to solve the inverse problem: what is the physical temperature profile that gives rise to the measured brightness temperature? This is an ill-posed problem and the solution is under-constrained.

Two different inversion methods have been used in this study. The temperature retrievals for the TEMPERA radiometer are based on the optimal estimation method (OEM) (Rodgers, 2000). The measured brightness temperatures are inverted to temperature profiles using the Atmospheric Radiative Transfer Simulator (ARTS)/QPack software package (Eriksson et al., 2011). More information about this method applied to TEMPERA measurements can be found in Stähli et al. (2013). For these retrievals, the absorption coefficients used in the radiative transfer calculations for the different species are obtained from the Rosenkranz and Liebe models: Rosenkranz (1993) for  $O_2$ , Liebe et al. (1993) for  $N_2$  and Rosenkranz (1998) for  $H_2O$ . A tropospheric water vapour profile is also included in the forward model. The profile is obtained from the measured surface water vapour density at the ground (from a weather station), assuming an exponential decrease of the water vapour with altitude and a scale height of 2 km (Bleisch et al., 2011). Standard atmospheric profiles for summer and winter are considered for other species such as oxygen and nitrogen (Anderson et al., 1986); these profiles are incorporated into ARTS2.

The retrievals for HATPRO measurements are based on a linear regression method. This algorithm uses simulated  $T_b$ s at required frequencies and elevation angles derived from 17 years of atmospheric radiosonde profiles at Payerne and radiative transfer calculations. The statistical multilinear regression coefficients are obtained from the comparison between the temperature profiles and the simulated  $T_b$ s' dataset from the radiosondes. For the HATPRO temperature retrievals, the brightness temperatures measured at the V-band frequencies are used, where the first three frequencies are only used in zenith pointing (51.26, 52.28 and 53.86 GHz), and the last four (54.94, 56.66, 57.3 and 58 GHz) are considered for all the elevation angles (Meunier et al., 2013). More details about the atmospheric profiles and the absorption models used in the radiative transfer model can be found in Löhnert and Maier (2012).

### 4 Brightness temperature comparison

The measured  $T_b$ s from both radiometers (TEMPERA and HATPRO) have been compared with the ones simulated using radiosonde (RS) measurements. The simulated  $T_b$ s from RSs were calculated using the Atmospheric Radiative Transfer Simulator (ARTS, Eriksson et al., 2011; Buehler et al., 2005), which implements the radiative transfer equation (RTE) presented in Eq. 1. In the radiative transfer calcu-

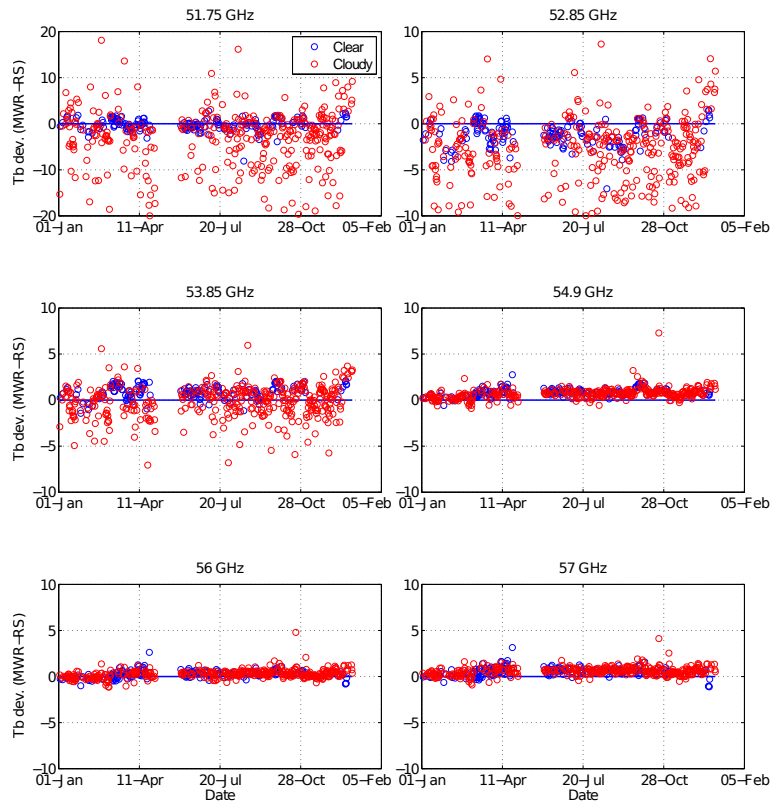


**Figure 3.** *T<sub>b</sub>* deviation between TEMPERA and RS at 60° elevation angle for six frequencies.

lations we use the models of Rosenkranz and Liebe for the absorption coefficient calculations: Rosenkranz (1998) for H<sub>2</sub>O, Rosenkranz (1993) for O<sub>2</sub> and Liebe et al. (1993) for N<sub>2</sub>. The input to the model consists of an atmospheric sounding, which provides information on pressure, height, temperature, water vapour density and cloud liquid water content (LWC). In this study we have assumed a constant LWC value of 0.28 g m<sup>-2</sup> for those altitudes with a relative humidity larger than 97 % and a temperature larger than -20 °C. As it was shown in Navas-Guzmán et al. (2014), this has a positive impact on the temperature retrievals from TEMPERA, while the shape of LWC profiles has a negligible impact. For other species like oxygen and nitrogen, we used standard atmospheric profiles for summer and winter (Anderson et al., 1986), which are incorporated into ARTS2.

In the next subsections we present the *T<sub>b</sub>* comparison for 1 year of measurements (January–December 2014) between the ones measured from TEMPERA and HATPRO radiometers and the simulated *T<sub>b</sub>* from RS measurements.

#### 4.1 TEMPERA vs. RS

In addition to atmospheric parameters, some radiometer characteristics were provided as input for the forward model. These input variables include the microwave frequencies, the elevation angles, the filter response and the antenna pattern.

Table 1 presents the central frequencies and the bandwidths of the different channels for TEMPERA. A Gaussian beam of 4° of half-power beamwidth (HPBW) has been considered as TEMPERA’s antenna pattern in the forward model.

The simulated *T<sub>b</sub>*s from RS measurements were calculated using ARTS model for the same elevations angles (12) and frequencies (9) as the ones used by TEMPERA in the tropospheric mode. A total of 532 measurements have been compared for 1 year of data.

Figure 3 shows the *T<sub>b</sub>* deviation between the TEMPERA radiometer and RSs at an elevation angle of 60° along 2014 for all weather conditions (except rainy cases). The classification of clear and cloudy cases was performed using an automatic partial cloud amount detection algorithm (AP-CADA) (Dürr and Philipona, 2004). This algorithm determines cloud fraction using long-wave downward radiation and surface temperature and humidity measurements with a 10 min resolution. The range goes from 0 octa (clear sky) to 8 octa (overcast). Clear conditions have been considered for those situations where the number of octas is 0 or 1. Moreover, an additional constraint considered was that the integrated liquid water (ILW) measured by the HATPRO radiometer was lower than 0.025 mm. We can observe in Fig. 3 that the largest bias in the *T<sub>b</sub>* between TEMPERA and RSs is found for the most transparent channels under cloudy conditions (red circles). For cloudy conditions there are discrep-

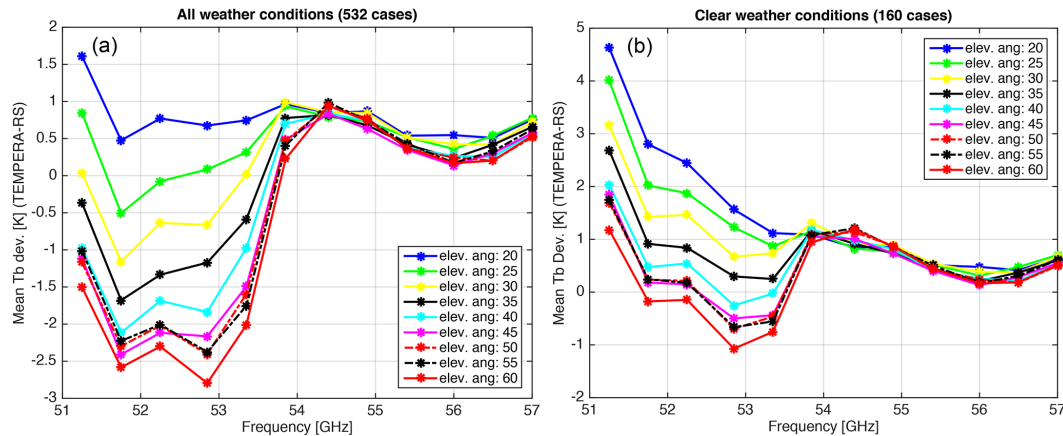


**Figure 4.** (a) Mean  $T_b$  deviation between TEMPERA and RS for all weather conditions (532 cases). (b) Mean  $T_b$  deviation between TEMPERA and RSs, only for clear conditions (160 cases).

ancies that reach almost 20 K for the 51.75 GHz channel. A different behaviour is observed for the most opaque channels where the bias between TEMPERA and RSs for both clear and cloudy conditions is much smaller, with deviations below 2 K for most of the measurements. The larger bias found for cloudy conditions can be explained by the presence of non-homogeneous conditions for many of the cases that produce incomparable measurements for both instruments. Moreover, the simulations of clouds in the forward model is an additional difficulty.

Figure 4a shows the mean  $T_b$  deviation between TEMPERA and RSs for all the frequencies and elevation angles of the TEMPERA radiometer and for all weather conditions. From this plot we can observe that there is a strong dependency on the frequency and the elevation angle. We could clearly separate the deviations between the transparent and the opaque channels. For the more opaque channels ( $> 53.5$  GHz) the agreement between TEMPERA and the RS is quite good, with differences always lower than 1 K for all the elevation angles. For these channels we can observe that there is no strong dependency on the elevation angles. In contrast, the more transparent channels show a strong dependency on the elevation angle and larger differences between TEMPERA and RS. The  $T_b$  bias ranges from positive values (1.6 K at 51.25 GHz) for the lowest elevation angle to negative values ( $-2.8$  K at 52.85 GHz) for the largest elevation angle. The change from positive to negative bias when the elevation angle increases could be due to the effect of the clouds in the forward model, suggesting a possible overestimation by the RS when clouds are incorporated into the forward model.

In order to avoid the complexity of cloudy cases which could present inhomogeneous conditions and to assess the  $T_b$  bias due to instrumental and modelling aspects, only cases with clear conditions were selected. Figure 4b shows the mean  $T_b$  deviation between TEMPERA and RS for clear

conditions. A total of 160 cases were identified as cloudless using the criteria mentioned above. From this plot we can also observe the strong dependency on the frequency and the elevation angle. The behaviour is similar to the plot with all weather conditions, finding the largest differences for the most transparent channels. For the more opaque channels ( $> 53.5$  GHz) the  $T_b$  bias ranges between 1.3 K (elev. angle of 30°, freq. of 53.85 GHz) and 0.2 K (elev. angle of 45°, freq. of 56 GHz). For the more transparent channels it is worth pointing out that for most of the channels and elevation angles there is a positive bias between the measured  $T_b$  from TEMPERA and the one simulated from RS. We can see that the bias is larger for the lower elevation angles. The bias ranges between 4.63 K (elev. angle of 20°, freq. of 51.25 GHz) and  $-1.1$  K (elev. angle of 60°, freq. of 52.85 GHz). In Table 2 we can find the mean  $T_b$  deviations and the standard deviations for five channels and all the elevations angles for clear conditions. Similar and even larger systematic offsets have been found in the more transparent V-band channels in other studies where radiometers from different manufacturers were used (Löhnert and Crewell, 2003; Hewison et al., 2006). The standard deviation of the  $T_b$  offsets (Table 2) is lower than 0.75 K for the channels that are more optically thick. However, the more transparent channels show standard deviations of the  $T_b$  offsets up to 1.73 K. The larger variability in the more transparent channels could be explained by a possible temporal shift between the radiosonde and the microwave radiometer (MWR) measurements since both techniques have different integration times and/or because both instruments sounded very different air masses (due to the vertical sonde drift). In addition, uncertainties in the oxygen absorption model as well as the radiometric noise could explain these variations (Löhnert and Maier, 2012).

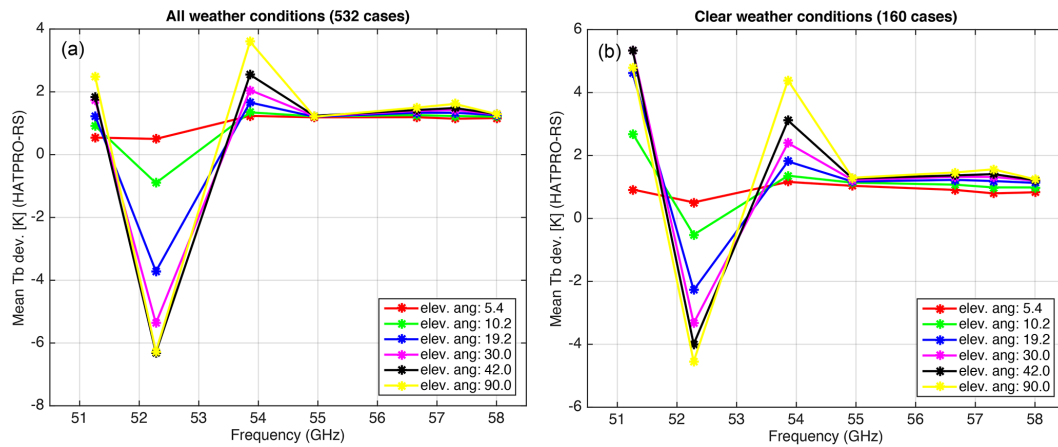


**Figure 5.** (a) Mean  $T_b$  deviation between HATPRO and RSs for all weather conditions (532 cases). (b) Mean  $T_b$  deviation between HATPRO and RSs, only for clear conditions (160 cases).

**Table 2.** Mean  $T_b$  and standard deviation between TEMPERA and RSs for clear conditions.

Elev. angle/freq.	51.25 GHz	52.25 GHz	53.35 GHz	54.90 GHz	56.50 GHz
20°	4.63/1.73	2.44/1.08	1.12/0.51	0.87/0.55	0.43/0.73
25°	4.01/1.70	1.87/1.26	0.87/0.61	0.77/0.51	0.49/0.68
30°	3.16/1.73	1.46/1.37	0.73/0.72	0.89/0.47	0.39/0.62
35°	2.69/1.67	0.84/1.41	0.25/0.80	0.73/0.45	0.40/0.58
40°	2.03/1.63	0.54/1.43	−0.03/0.89	0.81/0.45	0.24/0.56
45°	1.84/1.53	0.15/1.41	−0.44/0.95	0.73/0.44	0.32/0.54
50°	1.69/1.47	0.21/1.40	−0.46/0.99	0.88/0.42	0.22/0.50
55°	1.74/1.42	0.17/1.38	−0.56/0.99	0.85/0.43	0.35/0.51
60°	1.18/1.38	−0.15/1.36	−0.75/1.03	0.86/0.43	0.23/0.49

#### 4.2 HATPRO radiometer vs. RS

The  $T_b$  measured by the HATPRO radiometer was also compared with  $T_b$  simulated using RS measurements. For this new comparison the ARTS model was set with the radiometer instrument characteristics from HATPRO. The seven frequencies (51.26, 52.28, 53.86, 54.94, 56.66, 57.30 and 58.00 GHz) and the six elevation angles (90.0, 42.0, 30.0, 19.2, 10.2 and 5.4) of HATPRO were used as input for the forward model. The simulations were performed considering a pencil beam since the HPBW at the V-band frequencies for HATPRO is small ( $< 2.2^\circ$ ). In this study, the shape of the filter bandwidth is idealised to a rectangular function with the width specified by the manufacturer (230 MHz for the four most transparent channels, 600 MHz at 56.66 GHz, 1 GHz at 57.30 GHz and 2 GHz at 58 GHz).

Figure 5a shows the mean  $T_b$  deviations between HATPRO and RS for the seven frequencies and the six elevation angles of HATPRO radiometer. The plot presents the deviation for all weather conditions (532 cases). We can observe a positive  $T_b$  offset between HATPRO and the RS for all the frequencies and elevation angles except the second one (52.28 GHz). The  $T_b$  bias ranges between 3.6 K at 53.86 GHz

with the zenith pointing to  $-6.3$  K at 52.28 GHz and an elevation angle of  $42^\circ$ . In order to avoid possible inhomogeneous conditions due to the clouds, again we have selected clear cases for the comparison. Figure 5b shows the deviations for these conditions. We observe again that there is a strong dependency on the elevation angles for the more transparent channels, but in this case the second channel (52.28 GHz) evidences a very different behaviour than the other ones. A positive offset is observed in all the channels except for the second one. The  $T_b$  bias ranges between 5.3 K for the more transparent channels at  $30^\circ$  elevation angle and  $-4.5$  K for the second channel (52.28 GHz) at the zenith observation. For the more opaque channels ( $\geq 54.94$  GHz) the dependency on the elevation angle is weaker and shows a positive offset that ranges between 0.8 and 1.6 K.

Table 3 presents the mean and the standard deviation of the  $T_b$  differences between HATPRO and the radiosondes for the more transparent channels and all elevation angles. The largest standard deviation (2.1 K) is found for the most transparent channel at an elevation angle of  $19.2^\circ$ . A similar comparison study between the same radiometer and RS was performed by Löhnert and Maier (2012) for more than 3 years of measurements at Payerne. We would like to point out that

**Table 3.** Mean  $T_b$  and standard deviation between HATPRO and RSs for clear conditions.

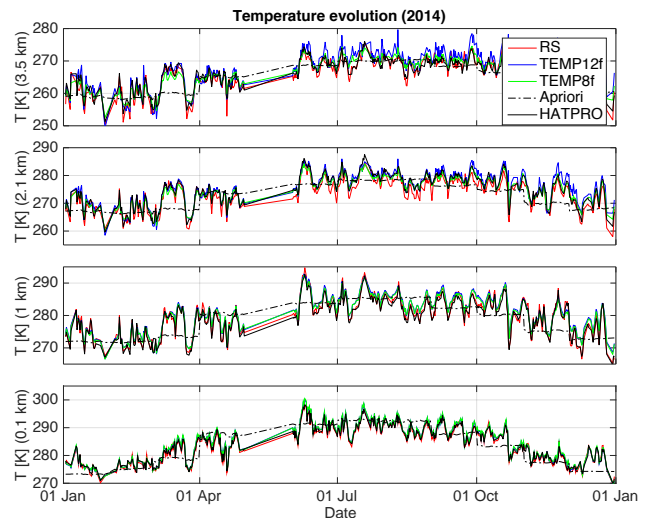
Elev. angle/freq.	51.26 GHz	52.28 GHz	53.86 GHz	54.94 GHz
5.4°	0.92/0.68	0.51/0.37	1.16/0.53	1.04/0.73
10.2°	2.69/1.78	-0.52/0.84	1.36/0.38	1.14/0.53
19.2°	4.61/2.10	-2.28/1.47	1.81/0.34	1.17/0.39
30°	5.35/1.84	-3.33/1.56	2.40/0.46	1.22/0.34
42°	5.33/1.60	-4.00/1.51	3.11/0.62	1.27/0.35
90°	4.79/1.25	-4.55/1.31	4.39/0.85	1.29/0.40

the calibration procedure has been significantly improved in our study in order to avoid the  $T_b$  discontinuities found in the paper of Löhnert and Maier (2012) due to some problematic liquid nitrogen calibrations. In the updated calibration procedure a series of checks is performed before a new calibration is accepted. For example, the scene at 5° elevation angle and the cold load are measured before and after the calibrations. One can expect to find  $T_b$  close to ambient air temperature and the boiling point of liquid nitrogen for the most opaque channels. If this is not the case, the calibration is rejected. Comparison with radiosondes using a forward model is also performed after calibration. Similar mean and standard deviations were found for the more transparent channels in Löhnert and Maier (2012) (when the problematic periods were excluded) compared to our study. In contrast, the other channels presented lower mean  $T_b$  deviations than in this study for the different elevation angles. It is also worth remarking that the largest mean  $T_b$  deviations are found for the larger elevation angles (larger than 19°) for both studies. One of the possible reasons that could explain these large discrepancies (larger than for TEMPERA) is that for the HATPRO radiometer the exact centre frequencies and band passes are not known for the instruments analysed in this study (Löhnert and Maier, 2012). Meunier et al. (2013) studied the impact of the radiometer characteristics (e.g. antenna beam width and receiver bandwidth) on scanning radiometer measurements, and they found that an inappropriate characterisation of the bandwidth could lead to errors of up to 8 K in the V band. The errors are more important in the vicinity of absorption peaks.

## 5 Intercomparison of retrieved temperature profiles

Physical temperature profiles retrieved from both MWRs are also compared with independent in situ temperature measurements from RS for 1 year of data (2014). A total of 532 coincident cases were inverted corresponding to all weather conditions (except rainy cases). As it was already indicated in Sect. 3, different inversion algorithms were used to retrieve temperature profiles from the two radiometers.

The temperature retrievals for TEMPERA are based on the optimal estimation method (OEM) and have been performed using ARTS/qpack package (Eriksson et al., 2011).

**Figure 6.** Temperature evolution at different altitudes for RSs, HATPRO and TEMPERA (inversions with 8 and 12 filters), and the a priori temperature used for TEMPERA inversions.

The method needs an a priori temperature profile in order to constrain the solutions to physically meaningful results. As a priori profiles, monthly mean temperature profiles calculated from 18 years (1994–2011) of daytime radiosonde profiles at Payerne are used.

We would like to point out that this a priori profile has a small impact on the temperature retrievals when the measurement response (MR) is high (> 80%), as in our case for the range used for the comparison. It means that more than 80% of the information comes from the measurements and not from the a priori profile. The MR is calculated for a determined altitude as the area under the averaging kernels (Rodgers, 2000). We have estimated for a specific case that the differences in the retrieved temperature profiles are smaller than 0.6% when a simple linear decrease temperature profile with a lapse rate of  $6.5 \text{ K km}^{-1}$  is used as the a priori profile instead of the mean profile for January obtained from the radiosonde climatology. Two different retrievals have been obtained for the TEMPERA measurements. In the first retrievals, the brightness temperatures for all the frequencies (12 channels) were used, while in the second one, only the eight more opaque channels were considered (fre-

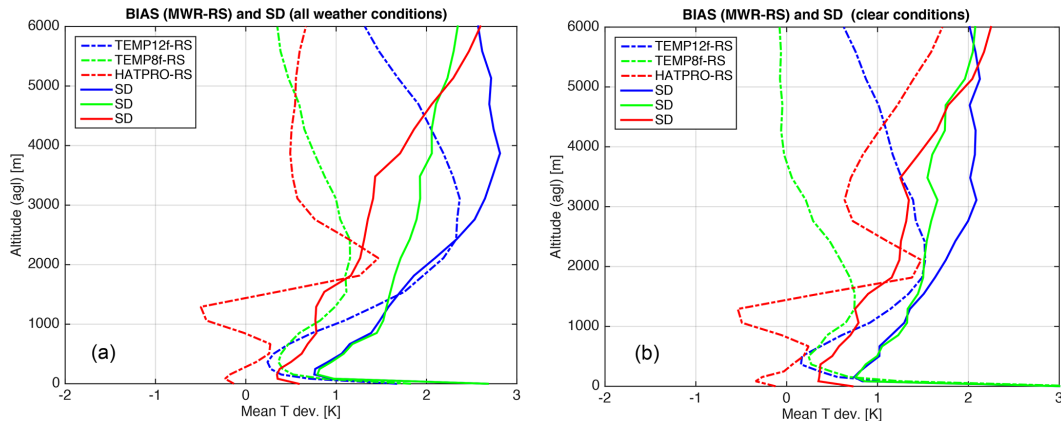


**Figure 7.** Mean (dashed-dotted lines) and standard temperature deviation (solid lines) between HATPRO/TEMPERA radiometers and RSs for all weather conditions (a) and clear skies (b).

quencies > 53 GHz). These two configurations were used in other studies to deal with clouds, only using the second retrievals (eight channels) when there was presence of clouds. It is well known that clouds have a relatively strong influence in the frequency range from 51 to 53 GHz (Stähli et al., 2013).

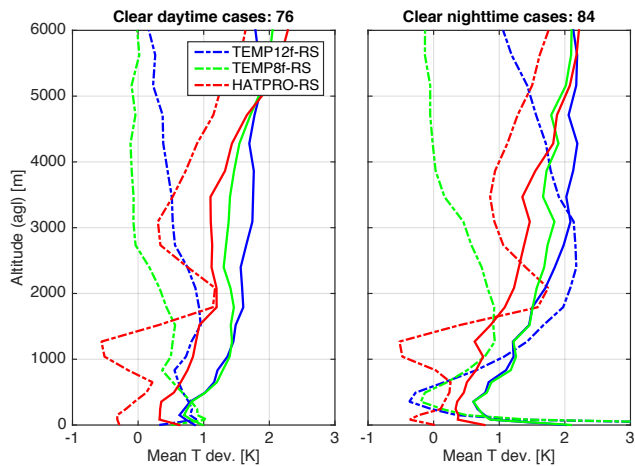
In order to perform the comparison between both radiometers and RSs, all the measurements have been interpolated to the altitude grid of TEMPERA. Figure 6 shows the temperature evolution for the RSs and TEMPERA (both inversions) and HATPRO radiometers at different altitudes along 2014. The a priori temperature used for the TEMPERA retrievals has also been plotted. We can observe that in general there is a very good agreement between RS and the retrievals from both radiometers. Both radiometers are able to follow the temperature evolution measured by the RS for the whole year, even if strong temperature changes are observed in a short time period. This plot shows the capability of MWR measurements to measure temperature profiles under very different atmospheric conditions. The highest discrepancies with the RSs are observed in the highest altitudes, particularly for the TEMPERA retrievals with 12 channels (blue line).

Figure 7a shows the bias and the standard deviation between the retrievals from both MWRs and the RS for all sky conditions. Very similar values of mean deviations are found between both retrievals from TEMPERA (with 8 and 12 channels) and the RS in the lowest troposphere (from 85 m to 1 km a.g.l.). Their values range between 0.24 and 0.86 K. For this altitude range the standard deviation also shows almost identical values, which range between 0.8 and 1.4 K. Larger offsets and standard deviations are found for both retrievals in the upper layers. The temperature deviation at ground level presents a larger deviation and is not considered in this discussion. This value could be improved for the future by considering the measurement from a temperature sensor co-located with TEMPERA as ground tem-

perature, as HATPRO radiometer does. Between 1 and 2 km above ground, the mean deviation shows very different values for the two retrievals. The one retrieved from eight channels (8f-RET) presents offsets between 0.8 and 1.1 K, while the one from 12 channels (12f-RET) evidences larger deviations (from 1.1 to 2 K). The standard deviations are also larger for the second retrievals, around 1.5 K for the 8f-RET and around 1.7 K for the 12f-RET. Above 2 km the bias for 8f-RET is much lower than the one for 12f-RET. The mean deviation ranges from 0.4 to 1.2 K and from 1.5 to 2.4, respectively, decreasing the offset with altitude and reaching a maximum deviation around 2.5 km above ground. The standard deviation increases with altitude in the range 2–6 km for both retrievals, with mean values of 1.9 K for the 8f-RET and 2.4 K for 12f-RET. From these results we can clearly observe a better agreement between the measurements from the radiosondes and the retrievals from TEMPERA when only the eight more opaque channels are used under all weather conditions.

Lower bias and standard deviations are found in the planetary boundary layer (PBL) for the retrievals from the HATPRO radiometer. The mean deviation ranges between  $-0.2$  and  $0.3$  K in the first kilometre and between  $-0.5$  and  $1.2$  K in the 1–2 km range altitude. Above 2 km the bias presents values between 0.5 and 1.5 K, showing a general decrease with altitude. The standard deviation shows an increase with altitude. The values range between 0.4 and 0.8 K in the first kilometre and 0.8 and 1.2 in the 1–2 km altitude range; there is a mean value of 1.5 K above 2 km.

In addition, we have assessed the accuracy of the retrievals only for clear sky conditions. The clear cases have been selected using the product APCADA and the ILW from HATPRO as has already been indicated in previous sections. A total of 160 temperature profiles have been compared. Figure 7b shows the bias and the standard deviation for clear cases. For TEMPERA retrievals we can observe that although the bias is almost the same than for all weather con-



**Figure 8.** Mean (dashed-dotted lines) and standard temperature deviation (solid lines) between HATPRO/TEMPERA radiometers and RSs during daytime (left) and night-time (right) under clear conditions.

dition in the first kilometre, there are lower deviations above this altitude for both retrievals. The mean deviations range from  $-0.03$  to  $0.7$  K and from  $1.2$  to  $1.5$  K in the altitude range between  $2$  and  $4$  km (a.g.l.), for 8f-RET and 12f-RET respectively. Above  $4$  km the bias is almost constant and close to zero ( $-0.1$  K) for the 8f-RET and shows a positive mean bias of  $0.9$  K for the 12f-RET. The standard deviations for both retrievals show very similar values in the lower part than for all weather conditions ( $0.9$  K of average in the first kilometre). Above this altitude the 8f-RET present lower standard deviation than 12f-RET ( $1.4$  K against  $1.6$  K between  $1$  and  $3$  km, and  $1.8$  K against  $2.1$  K between  $3$  and  $6$  km). These results also evidence a better agreement between RS and TEMPERA when only eight channels are used in the inversion algorithm although only clear cases have been selected. It could be explained for the larger  $T_b$  bias found for the most transparent channels under clear conditions.

The temperature comparison between HATPRO and RS under clear conditions shows almost identical values in the lowest part (from ground to  $3$  km) with respect to all weather conditions. The bias in this altitude range moves from  $-0.5$  K at  $1.3$  km to  $1.5$  K at  $2.1$  km (a.g.l.). Above  $3$  km (a.g.l.) the mean bias is  $1.3$  K.

It is worth pointing out that the bias for 8f-RET from TEMPERA shows lower values than for HATPRO above  $1.6$  km (a.g.l.), although the standard deviation is slightly lower for HATPRO almost in the whole range.

We have classified the measurements between day and night cases in order to check if there was any diurnal dependence. Figure 8 shows the bias and standard deviation for day (left) and night (right) measurements. We can observe that the standard deviations are very similar for all the retrievals in the lower troposphere (from ground to  $2$  km a.g.l.) during

the daytime and night-time. Slightly lower standard deviations are found above  $2$  km (a.g.l.) for the daytime retrievals from the two radiometers. In the case of the bias we can find some remarkable differences between day and night. We can observe a clear decrease in the bias for the retrievals from TEMPERA for daytime measurements. This is more evident in the case of the 12f-RET, changing the maximum bias from  $2.2$  K for night-time to  $0.9$  K for daytime. For the 8f-RET the decrease in the bias is also remarkable in the altitude range from  $1$  to  $4$  km (a.g.l.). For this range, the mean deviation is  $0.63$  K during night-time, while it reaches a mean value of  $0.22$  K during daytime.

It is worth mentioning that the differences between daytime and night-time deviations are much smaller for the retrievals from HATPRO. It could be explained by the fact that the inversion algorithm used for this radiometer is also very well trained for night-time measurements, since the regression method was also trained with radiosondes launched during night-time. The main remarkable atmospheric condition that can be found during the night is the presence of inversions. Therefore, the results evidence a larger difficulty for the retrievals from TEMPERA, especially for the 12f-RET, under the presence of inversion layers. Moreover, the fact that the a priori profiles for the TEMPERA retrievals have been calculated from a climatology using daytime radiosonde profiles could also explain some differences, and it is something that need to be investigated. Although the impact of the a priori profile on the retrieved temperature is small when the measurement response is high, it could be not negligible. Löhnert and Maier (2012) also found discrepancies in the temperature bias during daytime and night-time. They found a non-zero behaviour as a function of height with opposite sign between both datasets. It is important to note that the temperature bias values found in that study for HATPRO were lower than the ones observed in this work. It could be explained by the application of a  $T_b$  offset correction to that analysis.

## 6 Instrumental characteristic effect on microwave measurements

In this last section we assess the effect of instrumental characteristics such as the bandwidth of the individual filters and the antenna response on the brightness temperature.

Figure 9 presents the possible errors caused by omitting the antenna pattern from measurement simulations. The  $T_b$  bias has been defined as the  $T_b$  calculated from ARTS model considering a pencil beam minus the simulated  $T_b$  including a beam width. The antenna pattern was considered simulating a Gaussian response with a different HPBW (from  $1$  to  $8^\circ$ ). The simulations have been calculated for the 12 frequencies of TEMPERA and a set of elevation angles that covers the observational angles of both radiometers. From this plot we can observe that there is a strong dependency on fre-

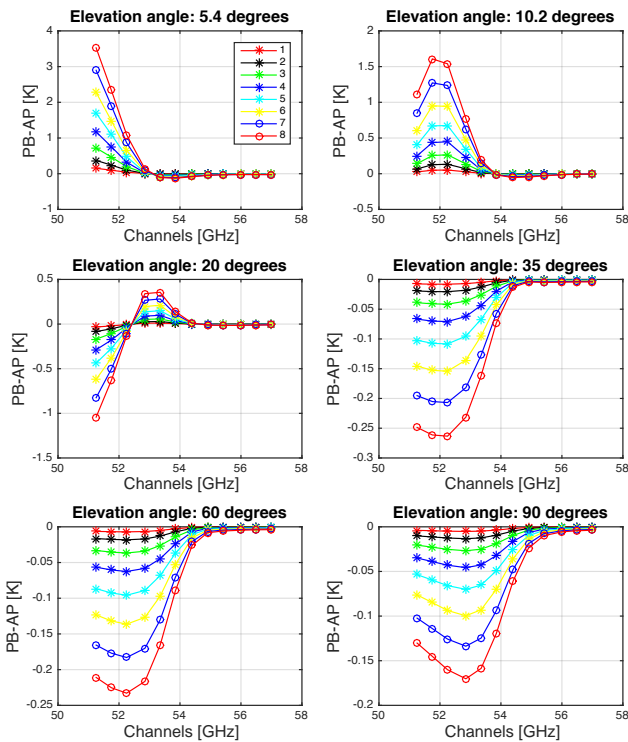


**Figure 9.** Errors associated with the antenna beam for different frequencies and elevation angles. The antenna beam was considered simulating a Gaussian response with a different HPBW (from 1 to 8°). The biases have been calculated as the  $T_b$ s considering the pencil beam (PB) minus the  $T_b$ s assuming different antenna patterns (AP).

quency and the elevation angle. For the more opaque channels (> 55 GHz) the brightness temperatures saturate and the errors associated with the antenna pattern can be considered negligible. The effect of the antenna pattern is more evident for the most transparent channels. The errors are larger when a larger HPBW is considered to characterise the antenna response. Next we will mention the errors associated with a HPBW of 4°, since the typical scanning radiometers used in the V band have this or smaller beam widths. The smallest errors are found for the zenith observations, with a maximum bias of -0.05 K at the frequency of 52.85 GHz. We can observe a similar behaviour but with a larger underestimation for lower elevation angles (up to 35°); at this angle the maximum bias reaches values of -0.07 K. We can observe that the deviations are much larger when a wider beam width is considered.

For the elevation angle of 20° we observe a change in the tendency of the bias, where we can find an underestimation for the most transparent channels (lower 52.5 GHz) and an overestimation above this frequency. The errors range between -0.3 and +0.1 K. This change from negative to positive bias for the elevation angle was also observed by Meu-

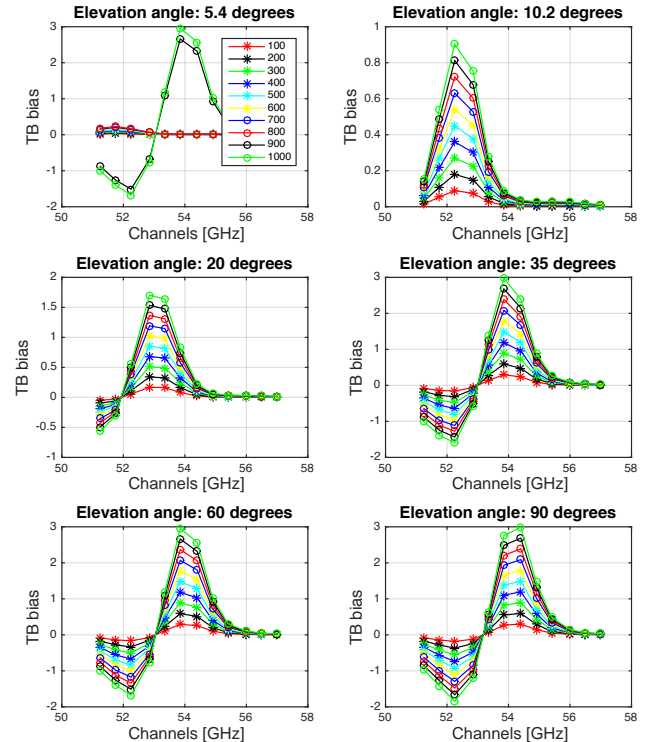


**Figure 10.** Errors associated with the bandwidth for different frequencies and elevation angles. The biases have been calculated as the  $T_b$ s considering the monochromatic receiver minus the  $T_b$ s assuming different bandwidths (from 100 to 1000 MHz).

nier et al. (2013), and it is linked to a change in the curvature of the  $T_b$  vs. angle curve.

The errors become larger for lower elevation angles. A maximum overestimation of 0.4 K is found at 52.75 GHz for the elevation angle of 10.2°. The maximum errors are found in the lowest elevation angle with a bias that reaches 1.2 K in the most transparent channel. For this angle, it is worth pointing out that the bias can reach values up to 3.5 K for a beam width with 8° of HPBW. The larger deviation for the lowest elevation angle (5.4°) could be explained by the beam at least partially hitting the ground (Meunier et al., 2013).

Figure 10 shows errors associated with the channel bandwidth effect in  $T_b$  differences for different elevation angles. The bias has been calculated as the  $T_b$  from ARTS model considering the monochromatic receiver minus the simulated  $T_b$  considering different bandwidths (from 100 to 1000 MHz) and assuming a rectangular response. The 12 central frequencies used for the simulations were the ones corresponding to TEMPERA’s channels. From the plot we can clearly observe that the bandwidth effect is very small when the opacity is high, so it corresponds to frequencies above 55 GHz at all elevation angles. In contrast, the bandwidth can have an important effect on most transparent channels. A general feature observed from these simulations is the existence of an overestimation, which moves up in frequency

when the elevation angle increases. The maximum biases are found for the widest bandwidths, and their values range between 0.9 and 3 K. This overestimation can be explained by the positive curvature of the  $Tb$  spectrum existing for frequencies lower than in the saturation range (Fig. 2). Similar behaviour has been observed by Meunier et al. (2013).

For elevation angles larger than  $10.2^\circ$  we observe an underestimation present in most of the transparent channels. These negative biases reach the maximum values again for the widest bandwidth ranging from  $-0.6$  K at  $20^\circ$  elevation angle to  $-1.8$  K at the zenith observation. These negative biases are related to the negative  $Tb$  curve for the most transparent channels present when the opacity is not very high (larger elevation angles).

It is worth pointing out the large bias observed for the two widest bandwidths (900 MHz and 1 GHz) at  $5.4^\circ$  elevation angle. While the narrower bandwidths show deviations smaller than 0.2 K, the widest ones reach biases that range between  $-1.7$  and 3 K.

Meunier et al. (2013) found that overestimations could reach values up to 8.5 and  $-2.5$  K of underestimation for some frequencies with the 1 GHz bandwidth. These large deviations are caused when the peaks of the oxygen individual absorption lines are also covered by the bandwidth of one of the channels. For this reason, it is very important that the central frequencies and the bandwidths of the different radiometer filters are not in the frequency range of any of the multiple absorption peaks.

## 7 Conclusions

This work presents an assessment of the tropospheric performance of a new temperature radiometer (TEMPERA). This is the first temperature radiometer that measures tropospheric and stratospheric temperature at the same time. In this study the measured brightness temperature and the retrieved tropospheric temperature are assessed by means of a comparison with simultaneous and collocated radiosonde measurements. In addition, the TEMPERA performances are compared with the ones from a commercial microwave radiometer (HATPRO), which has some different instrumental characteristics and uses a different inversion algorithm.

The measured brightness temperatures ( $Tbs$ ) from both radiometers (TEMPERA and HATPRO) have been compared with the ones simulated using radiosonde (RS) measurements. The simulated  $Tbs$  from RSs were calculated using the Atmospheric Radiative Transfer Simulator (ARTS). In general, much larger  $Tb$  deviations are found for the most transparent channels ( $< 54$  GHz) between the measured and the simulated  $Tbs$  from RSs for both radiometers. The deviations were much more pronounced for cloudy cases, where the bias reaches almost 20 K for some cases in the most transparent channels. The larger bias found for cloudy conditions could be due to cloud variability for many of the cases, which pro-

duces incomparable measurements between the different instruments. In addition, the assumption of a rectangular LWC profile with a value of  $0.28 \text{ g m}^{-3}$  to characterise the clouds is another source of errors.

In order to avoid the complexity of cloudy cases and to assess the effect due to instrumental and modelling aspects, only cases with clear conditions were selected. For these conditions, most TEMPERA channels showed a positive bias ranging from 4.63 K for the most transparent channel and the lowest elevation angle to  $-1.1$  K at a frequency of 52.85 GHz and the highest elevation angle ( $60^\circ$ ). The more opaque channels showed lower deviations ranging between 0.2 K and 1.3 K. Similar and even larger systematic offsets have been found in the more transparent V-band channels in other studies with radiometers from different manufacturers.

In the comparison between HATPRO and RSs, a similar pattern to the TEMPERA radiometer was found, with larger deviations for the most transparent channels. We observed a positive bias for all the frequencies and elevation angles except for the second channel (52.28 GHz). The positive bias ranged between 5.5 and 0.8 K. The large negative deviation found for the second channel, which reached values up to  $-4$  K, could be due to the fact that the central frequency defined for the model does not correspond to the actual centre frequency the instrument is measuring.

Comparison of the retrieved temperature profiles evidenced a good agreement in general between both radiometers and the independent in situ RS observations. Very similar values of mean deviations were found under all weather conditions between both retrievals calculated from TEMPERA measurements (with 8 and 12 channels) and the RS in the lowest troposphere (from 85 m to 1 km a.g.l.). The mean deviations were always lower than 0.86 K in this altitude range. Above 1 km lower mean deviations were found for 8f-RET with a maximum bias of 1.2 K, while for 12 f-RET the maximum mean deviation reached 2.4 K at 2.5 km. The standard deviations were very similar for both retrievals in the lower part but they increased with altitude, resulting in larger deviations for 12f-RET.

Lower bias and standard deviations were found in the PBL for the retrievals from the HATPRO radiometer. The mean deviation ranges between  $-0.2$  and 0.3 K in the first kilometre and between  $-0.5$  and 1.2 K in the 1–2 km range altitude. Above 2 km the bias presents values between 0.5 and 1.5 K, showing a general decrease with altitude. The standard deviation also shows an increase with altitude but with lower values than for TEMPERA retrievals.

For clear cases the bias and the standard deviations were very similar for all the retrievals in the lower part of the troposphere, while the most remarkable effect was a decrease in the bias for all the radiometer retrievals above 2 km. It is worth remarking that the lowest bias above this altitude was found for the 8f-TEMPERA retrievals with values always lower than 0.6 K. The standard deviations also decreased especially for the 12f-RET.

A classification of the temperature profiles between day and night observations evidenced a decrease in the bias and standard deviation for the daytime observations. It was especially important for the TEMPERA retrievals, which presented a lower bias than HATPRO in the far range (above 1.8 km). This comparison showed the good performance of HATPRO during night-time measurements, where normally the presence of more complex situations such as inversions, fog, etc. could be present. In this sense, the fact that the linear regression method of HATPRO was trained with a large dataset of night-time RS seems to be crucial. The temperature value for TEMPERA at the lowest altitude could be improved by incorporating a direct measurement of the ground temperature to the OEM algorithm and accounting for the correlation with higher altitudes.

It is worth pointing out the better agreement observed for TEMPERA when only the eight more opaque channels were used in the temperature retrievals, even under clear conditions. It could be due to the large  $T_b$  deviations observed in the most transparent channels, which are also observed in other studies that used different radiative transfer models. In this sense, future efforts should focus on the identification of the error sources of these uncertainties and in this way improve the performance of these most transparent channels. Instrumental characteristics such as the beamwidth and the bandwidth have been shown to have an important effect in the most transparent channels of the V band, reaching values of up to 3 K in the case of the bandwidth. However, they can not be considered as the source of the observed deviations in this study since they were considered in the simulations. Another possible explanation could also be that spectroscopy is not yet fully understood.

We conclude that this study has shown the good performance of the TEMPERA radiometer to determine the temperature in the troposphere. It is worth remarking the advantage of using the OEM for the TEMPERA retrievals, which does not have the disadvantage of needing to use a large RS database, as is the case for linear regression or neural network methods.

## 8 Data availability

Data used in this paper are available upon request to F. Navas-Guzmán (francisco.navas@iap.unibe.ch).

*Acknowledgements.* This work has been funded by the Swiss National Science Foundation under grant 200020-160048 and MeteoSwiss in the framework of the GAW project “Fundamental GAW Parameters by Microwave Radiometry”. The work has been also supported through the COST Action ES1303 (TOPROF), supported by COST (European Cooperation in Science and Technology) and by SBFI – contract no. C15.0030.

Edited by: D. Cimini

Reviewed by: two anonymous referees

## References

- Anderson, G. P., Clough, S., Kneizys, F., Chetwynd, J., and Shettle, E. P.: AFGL atmospheric constituent profiles (0.120 km), Tech. rep., DTIC Document, 1986.
- Bleisch, R., Kämpfer, N., and Haefele, A.: Retrieval of tropospheric water vapour by using spectra of a 22 GHz radiometer, *Atmos. Meas. Tech.*, 4, 1891–1903, doi:10.5194/amt-4-1891-2011, 2011.
- Buehler, S., Eriksson, P., Kuhn, T., Von Engeln, A., and Verdes, C.: ARTS, the atmospheric radiative transfer simulator, *J. Quant. Spectrosc. Ra.*, 91, 65–93, doi:10.1016/j.jqsrt.2004.05.051, 2005.
- Crewell, S. and Lohnert, U.: Accuracy of boundary layer temperature profiles retrieved with multifrequency multiangle microwave radiometry, *IEEE T. Geoscience Remote*, 45, 2195–2201, 2007.
- De Haan, S.: High-resolution wind and temperature observations from aircraft tracked by Mode-S air traffic control radar, *J. Geophys. Res.-Atmos.*, 116, D10111, doi:10.1029/2010JD015264, 2011.
- Dürr, B. and Philipona, R.: Automatic cloud amount detection by surface longwave downward radiation measurements, *J. Geophys. Res.-Atmos.* (1984–2012), 109, D05201, doi:10.1029/2003JD004182, 2004.
- Eriksson, P., Buehler, S., Davis, C., Emde, C., and Lemke, O.: ARTS, the atmospheric radiative transfer simulator, version 2, *J. Quant. Spectrosc. Ra.*, 112, 1551–1558, doi:10.1016/j.jqsrt.2011.03.001, 2011.
- Hewison, T. J., Cimini, D., Martin, L., Gaffard, C., and Nash, J.: Validating clear air absorption models using ground-based microwave radiometers and vice-versa, *Meteorol. Z.*, 15, 27–36, doi:10.1127/0941-2948/2006/0097, 2006.
- Liebe, H., Hufford, G., and Cotton, M.: Propagation modeling of moist air and suspended water/ice particles at frequencies below 1000 GHz, in: In AGARD, Atmospheric Propagation Effects Through Natural and Man-Made Obscurants for Visible to MM-Wave Radiation 11 p (SEE N94-30495 08-32), vol. 1, 1993.
- Löhnert, U. and Crewell, S.: Accuracy of cloud liquid water path from ground-based microwave radiometry 1. Dependency on cloud model statistics, *Radio Sci.*, 38, 8041, doi:10.1029/2002RS002654, 2003.
- Löhnert, U. and Maier, O.: Operational profiling of temperature using ground-based microwave radiometry at Payerne: prospects and challenges, *Atmos. Meas. Tech.*, 5, 1121–1134, doi:10.5194/amt-5-1121-2012, 2012.
- Martin, L., Schneebeli, M., and Matzler, C.: ASMUWARA, a ground-based radiometer system for tropospheric monitoring,

- Meteorol. Z., 15, 11–17, doi:10.1127/0941-2948/2006/0092, 2006.
- Meunier, V., Löhnert, U., Kollias, P., and Crewell, S.: Biases caused by the instrument bandwidth and beam width on simulated brightness temperature measurements from scanning microwave radiometers, *Atmos. Meas. Tech.*, 6, 1171–1187, doi:10.5194/amt-6-1171-2013, 2013.
- Navas-Guzmán, F., Stähli, O., and Kämpfer, N.: An integrated approach toward the incorporation of clouds in the temperature retrievals from microwave measurements, *Atmos. Meas. Tech.*, 7, 1619–1628, doi:10.5194/amt-7-1619-2014, 2014.
- Navas-Guzmán, F., Kämpfer, N., Murk, A., Larsson, R., Buehler, S. A., and Eriksson, P.: Zeeman effect in atmospheric O<sub>2</sub> measured by ground-based microwave radiometry, *Atmos. Meas. Tech.*, 8, 1863–1874, doi:10.5194/amt-8-1863-2015, 2015.
- Rodgers, C. D.: Inverse methods for atmospheric sounding: Theory and Practice, Series on Atmospheric, Oceanic and Planetary Physics, Vol. 2, World Scientific, 2000.
- Rose, T., Crewell, S., Löhnert, U., and Simmer, C.: A network suitable microwave radiometer for operational monitoring of the cloudy atmosphere, *Atmos. Res.*, 75, 183–200, doi:10.1016/j.atmosres.2004.12.005, 2005.
- Rosenkranz, P. W.: Absorption of microwaves by atmospheric gases, in: *Atmospheric remote sensing by microwave radiometry*, edited by: Janssen, M. A., John Wiley & Sons, 37–90, 1993.
- Rosenkranz, P. W.: Water vapor microwave continuum absorption: A comparison of measurements and models, *Radio Sci.*, 33, 919–928, doi:10.1029/98RS01182, 1998.
- Stähli, O., Murk, A., Kämpfer, N., Mätzler, C., and Eriksson, P.: Microwave radiometer to retrieve temperature profiles from the surface to the stratopause, *Atmos. Meas. Tech.*, 6, 2477–2494, doi:10.5194/amt-6-2477-2013, 2013.
- Ware, R., Carpenter, R., Güldner, J., Liljegren, J., Nehr Korn, T., Solheim, F., and Vandenberghe, F.: A multichannel radiometric profiler of temperature, humidity, and cloud liquid, *Radio Sci.*, 38, 8079, doi:10.1029/2002RS002856, 2003.